Solid State Communications 251 (2017) 10–15

Contents lists available at ScienceDirect

Solid State Communications

journal homepage: www.elsevier.com/locate/ssc

Communication

Hybrid graphene-BC_2N monolayers and nanoribbons with extended line defects: An ab initio study

T. Guerra[a,*], S. Azevedo[a], M. Machado[b]

[a] Departamento de Física/CCEN, Universidade Federal da Paraíba, Caixa Postal 5008, 58051-900 João Pessoa, PB, Brazil
[b] Departamento de Física, Universidade Federal de Pelotas, Caixa Postal 354, 96010-900 Pelotas, RS, Brazil

A B S T R A C T

Opening a bandgap in graphene is probably one of the most important and urgent topics in the graphene research currently, since most of the proposed applications for graphene in nanoelectronic devices require the ability to adjust its bandgap. In this work we perform first-principles calculations to investigate the alterations at the structural, energetic, electronic and magnetic properties of hybrid graphene-BC_2N monolayers (GBMLs) and zigzag graphene-BC_2N nanoribbons (ZGBNRs) with different types of extended line defects (ELDs) at the grain boundary. Different reconstruction processes are observed forming different types of ELDs depending on the nature of the atoms into the grain boundary as well as the structures type, arrangement, position/size of domains, and inserted atoms. The inclusion of these ELDs creates edge type effects in the ELD at GBNMLs, inducing spin polarization and localization of states at the Fermi level. GBNMLs show a wide range of electronic structures going from semimetallic to semiconducting and metallic, which can have magnetic ground states with ferromagnetic and antiferromagnetic. ZGBNRs are always metallic with ferromagnetic coupling between carbon atoms at the structures edges.

1. Introduction

Graphene [1] has been called the material of the 21st century because of its exceptional physical [2], electronic [3], optical [4], and mechanical [5] properties. This two-dimensional (2D) material formed only by carbon (C) atoms, presenting sp^2 hybridization, honeycomb lattice, zero energy gap and a null density of states at the Fermi level, conducts electricity ten times better than expected [6]. It is the thinnest compound known to man at one atom thick, mechanically very strong, flexible, absorbing 2.3% of white light and presenting high electronic mobility at room temperature [7,8]. Several researchers have struggled to fabricate the graphene into ultra-narrow strips [9], called graphene nanoribbons (GNRs) with extraordinary electronic and magnetic properties [10–13]. Depending on the way the cut is performed the GNRs can present different forms, widths and edge types known as armchair graphene nanoribbons (AGNRs) or zigzag graphene nanoribbons (ZGNRs) [14].

Hexagonal boron nitride monolayer (BNML) is a synthetic material, presenting a honeycomb configuration, equal number of boron (B) and nitrogen (N) atoms at its structure and sp^2 hybridization, very similar to the one shown by the graphene [15]. It is an indirect wide bandgap semiconductor (5.955 eV) with very high thermal and chemical stability, being used in devices operating under extreme conditions [16]. BN nanoribbons (BNNRs) shows exotic electronic structure and magnetic properties [17–19].

Since the C and BN honeycombed structures are structurally similar, hybrids of C and BN have attracted the scientific interest due to the possibility to obtain nanomaterial with intermediate properties between graphene and boron nitride systems. One of these structures is the BC_2N, which have been synthesized using different experimental methods [20–22]. There are several possible atomic arrangements for a BC_2N monolayer. Li et al. calculated the electronic properties of such structures and found that two of the structural models for BC_2N are semiconductors, with indirect band gap of 1.6 and 0.5 eV, and the third one behaves as a metal [23]. Azevedo calculated the energetic properties of sixteen possible arrangements BC_2N, with gap ranging from 0 to 1.62 eV, and showed that stable structures are obtained by increasing the number of C-C and B-N bonds. Also, it was shown that the less stable structures result from the increasing number of N-N and B-B bonds [24]. In addition, it is interesting to point out that BC_2N nanoribbons (BC_2NNRs) also show a variety of electronic behaviours, including metallic, semiconducting and semi-metallic, which are dominated by the structures edge type and composition [25].

Graphene-BN hybrid structures, consisting of domains of graphene-BN can exist in various configurations [26,27]. Here, we report a first-principles study of hybrid graphene-BC_2N monolayers and

* Correspondence to: Department of Physics, Cidade Universitária, João Pessoa, Brazil.

http://dx.doi.org/10.1016/j.ssc.2016.12.005
Received 27 September 2016; Received in revised form 5 December 2016; Accepted 9 December 2016
Available online 13 December 2016
0038-1098/

nanoribbons with ELDs at the grain of boundaries in different positions, arrangements of domains, and different chemical species. Modification of graphene properties observed opens up new opportunities for nanoelectronic and spintronic applications.

2. Methodology

The calculations were performed using the Spanish Initiative for Electronic Simulations with Thousands of Atoms (SIESTA) code [28,29], which is used to predict physical properties such as electronic structure, spin polarization, energies, atomic forces, geometry optimization, local density of states, densities of state, charge and spin charge of atoms, molecules and solids. In this study we investigate the electronic, structural, energetic and magnetic properties of hybrid GBMLs and ZGBNRs with extended line defect. The SIESTA performs full self-consistent calculations within the density functional theory (DFT) [30] solving the Kohn-Sham equations for the electrons using a basis set of numerical atomic orbitals in the generalized gradient approximation (GGA) [31] with the exchange and correlation terms parametrized for Perdew-Burke-Ernzerhof (PBE) [32]. The interactions between electrons and core are described by non-local norm-conserving Troullier-Martins pseudopotential [33] factorized in the Kleinman-Bylander form [34] and a double-ζ polarized (DZP) basis set composed by numeric atomic orbitals with a cuttoff radius of ≈15.0 Å. In the calculations, only the valence orbitals were treated self-consistently. The valence configuration for the construction of pseudopotentials are chosen as $1s^1$, $2s^22p^1$, $2s^22p^2$ and $2s^22p^3$ for H, B, C and N respectively. All of the geometries were optimized using the conjugate gradient method until the residual Hellmann-Feynman forces acting on any atom were smaller than 0.1 eV/Å. We adopt a rectangular supercell where the monolayers (MLs) and nanoribbons (NRs) have same sizes and numbers of atoms for each model. The calculations were performed at absolute zero and in vacuum. The systems studied, after optimization, can be seen at Fig. 1. Here, we use the label $GBML_{(ELD)\ D(GB)}$ to represent a hybrid graphene-BC_2N monolayer with one ELD formed by octagonal or tetragonal rings (8 or 4), with atoms deposited (D) at the grain boundaries of graphene-BC_2N and having different BC_2N domains, with each domain characterized by the species in the grain boundary (GB).

The calculation of the energetic stability of various GBMLs and ZGBNRs is performed using a zero-temperature approach based on the prior determination of convenient chemical potentials, as described in [35–37]. In this approach, the formation energy by atom (E_{for}) can be written as:

$$E_{for} = (E_{tot} - n_B\mu_B - n_C\mu_C - n_N\mu_N - n_{HB}\mu_{HB} - n_{HC}\mu_{HC} - n_{HN}\mu_{HN})/n_t, \quad (1)$$

where E_{tot} is the calculated total energy, n_C, n_B, n_N, n_{HB}, n_{HC}, and n_{HN} are the number of C, B, N atoms, and H-B, H-C and H-N bonds, respectively, μ_B, μ_C, μ_N, μ_{HB}, μ_{HC} and μ_{HN} are the respective theoretical chemical potentials, and n_t is the total number of atoms.

3. Results and discussion

3.1. Structural properties

Table 1 summarizes the obtained results of a comparative study about the formation energy of all calculated structures. It can be noticed that between GBMLs and ZGBNRs with ELDs, $GBML_{8BN}$ and $ZGBNR_{8BN}$ are the most stable structures. Both structures show a one-dimensional topological defect at the graphene - BC_2N interface, containing octagonal and pentagonal rings with sp^2 hybridization. This ELD composed by two pairs of pentagonal rings surrounding one octagonal ring (558-ELD) has been synthesized by different methods. Lahiri et al. have synthesized a 558-ELD with two different arrangements on a nickel substrate, inducing an atomic translation relative to each other [38] and more recently, Chen and co-workers have synthesized a 558-ELD using simultaneous electron irradiation and Joule heating by applied electric current [39].

Furthermore, the presence of B-B bonds separating pentagonal rings is observed. It is known that B atoms can have up to eight valence electrons, a pair in each of four orbitals. In atomic B, one of these orbitals is completely empty and the other three are half-full, with one electron apiece. Braunschweig et al. filled all four orbitals by bonding each B atom to a molecule that donated two electrons in a way that each B atom could completely fill its orbitals by pairing up with another B and pooling its original three electrons [40]. In our case, the four-coordinated B atom receives a pair of electrons of the N (lone pair) and the most stable systems, $GBML_{8BN}$ and $ZGBNR_{8BN}$, besides having a 558-ELD, also present the maximum number of B-N bonds.

Nozaki et al. [41] estimated the bond energies, ε, for the six possible pairs formed by B, C and N. It was shown that $\varepsilon_{BN} > \varepsilon_{CC} > \varepsilon_{CN} > \varepsilon_{CB} > \varepsilon_{BB} > \varepsilon_{NN}$, which indicates the hierarchy of the energetic stability of the B-N, C-C, C-N, C-B, B-B and N-N chemical bonds, respectively. This work demonstrates that the structures with maximum number of B-N bonds and 558-ELD ($GBML_{8BN}$ and $ZGBNR_{8BN}$) are the most energetically stable (see Fig. 1(c) and Table 1). The second and third most stable structure are $GBML_{8CN}$ and $ZGBNR_{8CN}$ and $GBML_{8NC}$ and $ZGBNR_{8NC}$, respectively. These structures are shown in Fig. 1(a) and (e), respectively. They also have a 558-ELD and obey the law that indicates the hierarchy of the energetic stability previously mentioned. In general, the most stable structures are those which maximize the number of B-N or C-C bonds and present a 558-ELD.

Moreover, it was found that the GBMLs and GBNRs with the higher formation energies correspond to those structures which present the extended line defect formed by tetragonal carbon rings (4-ELD). Li and colleagues have proposed a way to generate one stable 4-ELD at graphene [42]. The incorporation, at GBMLs and ZGBNRs, of a flat 4-ELD, with the middle carbon atoms presenting a sp^3-like hybridization has high energetic cost, as can be seen in Table 1. Structures that have higher formation energies ($GBML_{4CC}$ and $GBML_{4CN}$) can be seen in Fig. 1(g) and (j), respectively. They show a 4-ELD with the carbon atoms remaining (flat) at the plane, being four coordinated and strongly confined between the atoms of the 4-ELD, resulting into the high value for the formation energies.

The structures $GBML_{4NN}$ and $ZGBNR_{4NN}$ and $GBML_{4NC}$ and $ZGBNR_{4NC}$, as seen at Fig. 1(h) and (k), respectively, should have 4-ELDs. However, we observe the formation of 558 and 8-ELD. This happens because the number of electrons at the grain boundaries influences the reconstruction process of the ELDs, i.e., whether it is electron rich (or poor) there is facility (or difficulty) for the atoms to move out (or in) of plane [43].

3.2. Magnetic properties

Here, we perform a comparative analysis of magnetic moment by supercell (μ) of all studied structures. Magnetic moment in graphene can be induced by removing a single p_z orbital. Because of the bipartite atomic structure of graphene, labeled A and B, according to Lieb's theorem [44], the ground state of the system possesses a total spin given by $S = 1/2|N_A - N_B|$, where N_A and N_B are the number of p_z orbitals removed from each sublattice. Thus, to generate a net magnetic moment in a particular graphene region, a different number of p_z orbitals from each sublattice needs to be locally removed [45].

As shown in Table 1 and Fig. 2(a), the $GBML_{8CN}$ and $ZGBNR_{8CN}$ present net magnetic moment due to the presence of a pentagonal carbon ring, for the $GBML_{8CN}$, and a carbon atom at the zigzag edge, for $ZGBNR_{8CN}$. On the other hand, at Fig. 2(d) the existence of two pentagonal carbon rings results at no pending bond and null magnetic moment. All ZGBNRs show magnetic moment localized at the C edge atoms: since C atoms with sp^2 hybridization have a p_z orbital contain-

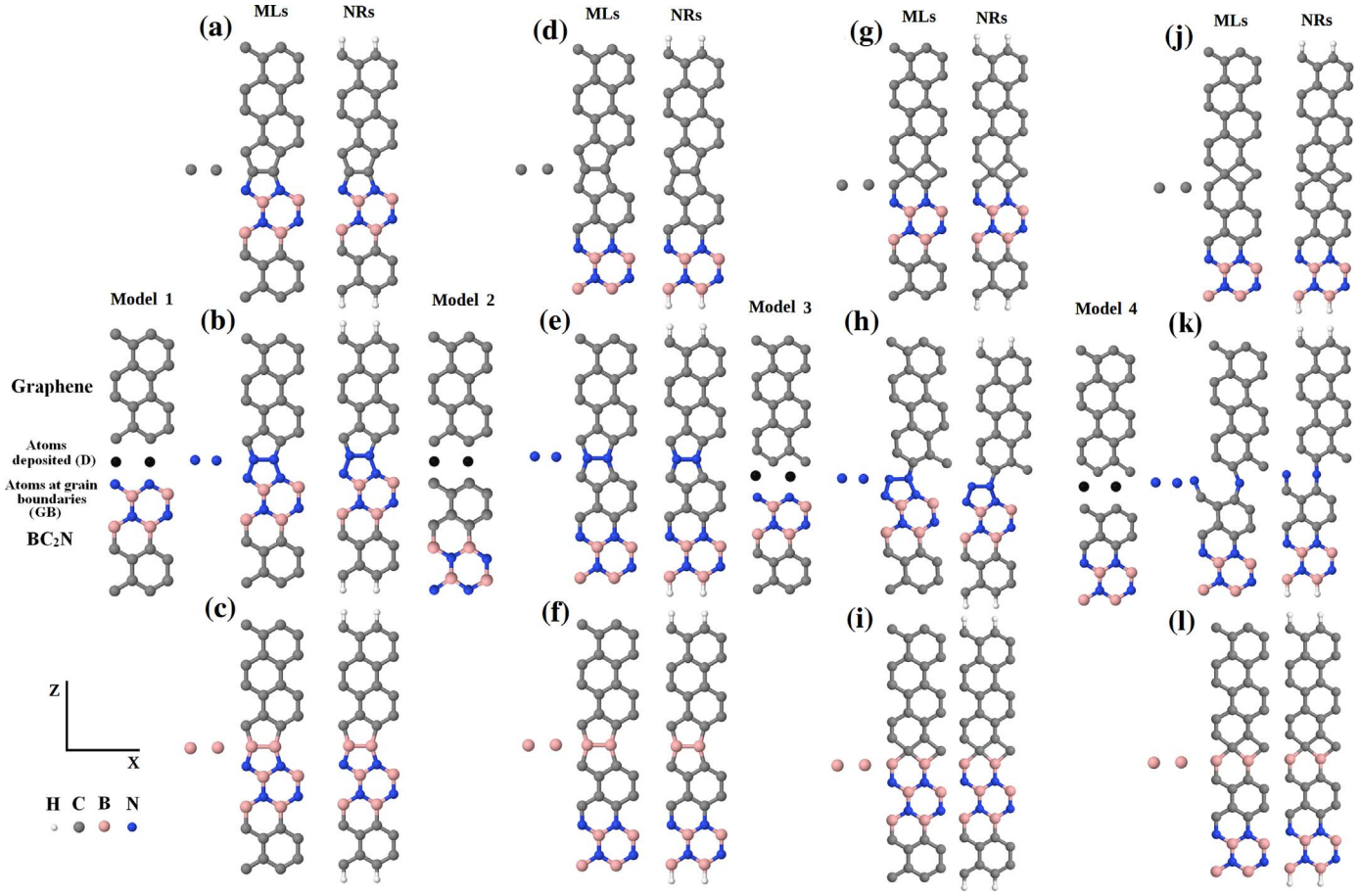

Fig. 1. Pictorial scheme for the studied hybrid graphene-BC_2N monolayers and nanoribbons after optimization, with extended line defects (ELDs) formed by octagonal or tetragonal rings (8 or 4), depositing of different chemical species (D) at the grain boundaries of graphene-BC_2N and having different BC_2N domains, with each domain characterized by species in the grain boundary (GB). In this manner, the studied structures will be labeled according to the following scheme: $GBML_{(ELD)(D)(GB)}$ and $ZGBNR_{(ELD)\ (D)\ (GB)}$. There are four proposed models, **Model 1**: (a) ($GBML_{8CN}$ and $ZGBNR_{8CN}$), (b) ($GBML_{8NN}$ and $ZGNR_{8NN}$), (c) ($GBML_{8BN}$ and $ZGBNR_{8BN}$); **Model 2**: (d) ($GBML_{8CC}$ and $ZGBNR_{8CC}$), (e) ($GBML_{8NC}$ and $ZGBNR_{8NC}$), (f) ($GBML_{8BC}$ and $ZGBNR_{8BC}$); **Model 3**: (g) ($GBML_{4CN}$ and $ZGBNR_{4CN}$), (h) ($GBML_{4NN}$ and $ZGBNR_{4NN}$), (i) ($GBML_{4BN}$ and $ZGBNR_{4BN}$); **Model 4**: (j) ($GBML_{4CC}$ and $ZGBNR_{4CC}$), (k) ($GBML_{4NC}$ and $ZGBNR_{4NC}$), (l) ($GBML_{4BC}$ and $ZGBNR_{4BC}$). Hydrogen, boron, carbon and nitrogen atoms are represented by the white, light pink, gray, and dark blue spheres, respectively. Atoms deposited (adatoms) are represented by black spheres. (For interpretation of the references to color in this figure legend, the reader is referred to the web version of this article.)

ing one electron which is oriented perpendicularly to the structure plane and, as the edge carbons atoms make only three single bonds, they have a free electron that results in the observed net magnetic moment. The p_z orbital of the B atoms remain vacant, whereas the corresponding p_z orbital of the N atoms are occupied by two electrons. At Figs. 2(b), (e), (f), (h), and (k) we have one or two lines of N or B atoms, generating some type of an edge in the ELD at GBNMLs, but, as all C atoms in these structures are four coordinated, there are not free electrons and the net magnetic moment is null. At Fig. 2(c) we have a line of B atoms, which receive the N atoms lone pairs, with the remaining electrons being transferred to the C atoms, due to its higher electronegativity. Finally, at Figs. 2(g), (i), (j) and (l) we see that the line of C atoms with sp^3 hybridization introduces edge effects in ELD with pending bonds and a non null net magnetic moment.

For GBMLs, the number of carbon atoms in each sublattice for the graphene and BC_2N domains are equal. However, with the atom

Table 1
Formation energy (E_{for}), the magnetic moment by supercell (μ), ground state spin configuration (G), band gap (eV) and type of extended line defects for the studied systems after optimization.

Structures	E_{for} (eV)	μ (μ_B)	G	Gap (eV)	Type of ELD
$GBML_{8CN}$/**$ZGBNR_{8CN}$**	0.13/ **0.13**	0.39/ **1.00**	FM/ **FM**	0.00/ **0.00**	558/ **558**
$GBML_{8NN}$/**$ZGBNR_{8NN}$**	0.19/ **0.18**	0.00/ **0.64**	AFM/ **FM**	0.50/ **0.00**	558/ **558**
$GBML_{8BN}$/**$ZGBNR_{8BN}$**	0.12/ **0.12**	0.88/ **0.90**	FM/ **FM**	0.00/ **0.00**	558/ **558**
$GBML_{8CC}$/**$ZGBNR_{8CC}$**	0.14/ **0.14**	0.00/ **0.23**	AFM/ **FM**	0.10/ **0.00**	558/ **558**
$GBML_{8NC}$/**$ZGBNR_{8NC}$**	0.13/ **0.13**	0.00/ **0.85**	AFM/ **FM**	0.20/ **0.00**	558/ **558**
$GBML_{8BC}$/**$ZGBNR_{8BC}$**	0.18/ **0.18**	0.00/ **0.54**	AFM/ **FM**	0.20/ **0.00**	558/ **558**
$GBML_{4CN}$/**$ZGBNR_{4CN}$**	0.38/ **0.34**	0.16/ **1.29**	FM/ **FM**	0.00/ **0.00**	4/ **4**
$GBML_{4NN}$/**$ZGBNR_{4NN}$**	0.21/ **0.17**	0.00/ **0.57**	AFM/ **FM**	0.00/ **0.00**	558/ **558**
$GBML_{4BN}$/**$ZGBNR_{4BN}$**	0.21/ **0.20**	0.78/ **1.39**	FM/ **FM**	0.00/ **0.00**	4/ **4**
$GBML_{4CC}$/**$ZGBNR_{4CC}$**	0.39/ **0.27**	0.11/ **0.69**	FM/ **FM**	0.00/ **0.00**	4/ **4**
$GBML_{4NC}$/**$ZGBNR_{4NC}$**	0.17/ **0.14**	0.00/ **0.90**	AFM/ **FM**	0.10/ **0.00**	558/ **8**
$GBML_{4BC}$/**$ZGBNR_{4BC}$**	0.26/ **0.22**	0.53/ **2.00**	FM/ **FM**	0.00/ **0.00**	4/ **4**

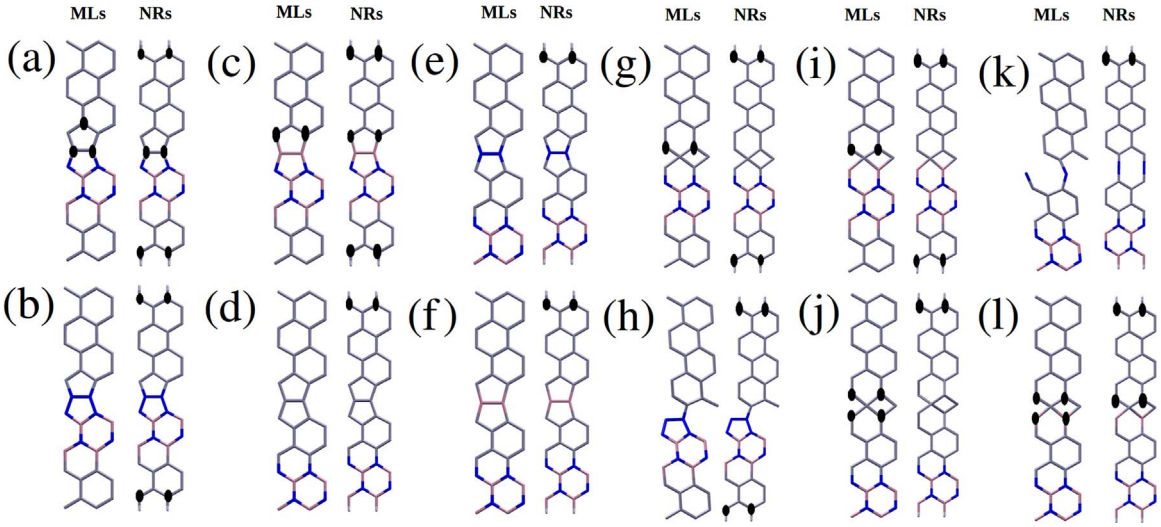

Fig. 2. Net spin-charge density represented by isosurfaces black at supercell for studied GBMLs and ZGBNRs.

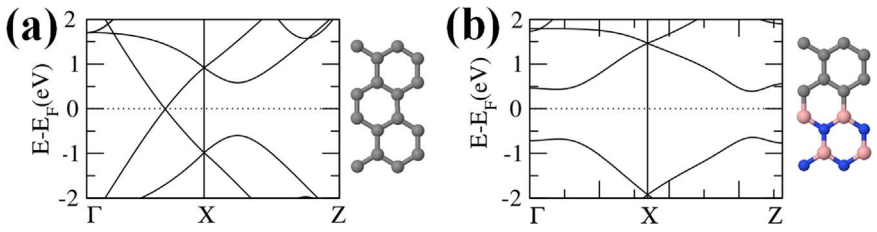

Fig. 3. Band structures of graphene (GML) (a) and BC_2N (BC_2NML) (b) monolayers.

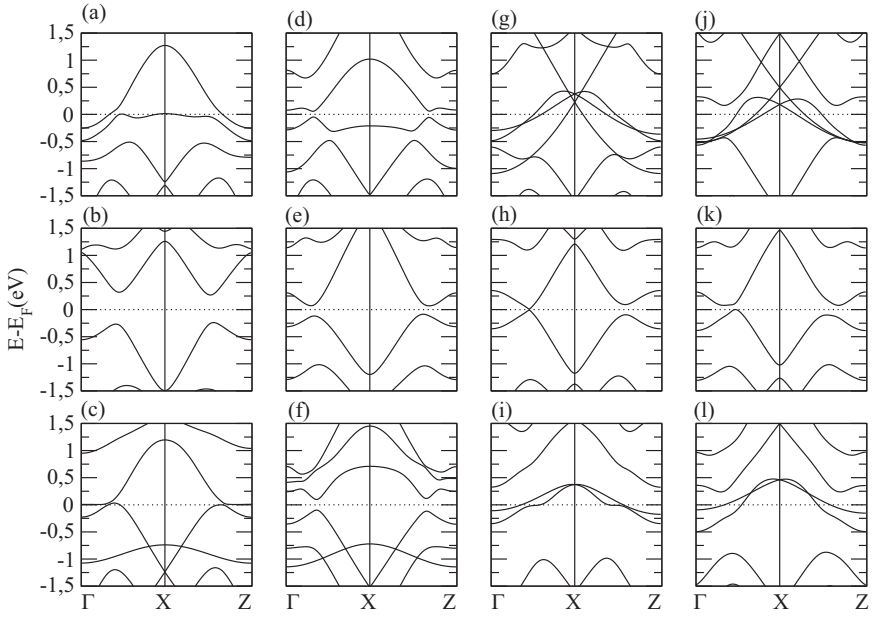

Fig. 4. Band structures of all GBMLs studied: (a) $GBML_{8CN}$, (b) $GBML_{8NN}$, (c) $GBML_{8BN}$, (d) $GBML_{8CC}$, (e) $GBML_{8NC}$, (f) $GBML_{8BC}$, (g) $GBML_{4CN}$, (h) $GBML_{4NN}$, (i) $GBML_{4BN}$, (j) $GBML_{4CC}$, (k) $GBML_{4NC}$ and (l) $GBML_{4BC}$.

insertion in the grain boundaries, the number of carbon atoms between the different sublattices (or p_z orbitals) can be either balanced or unbalanced, generating either a null or non null magnetic moment.

3.3. Electronic properties

Fig. 3 shows the calculated band structures of graphene (GML) and BC_2N (BC_2NML) monolayers. Graphene is a semimetal (zero-gap semiconductor) with null density of states at the Fermi level [3]. The more stable BC_2NMLs, have an energy gap ranging from 0 to 1.62 eV [24]. Our system, Fig. 3(b), is a semiconductor with band gap of about 1 eV. Is expected that all studied structures illustrated in Fig. 1 would have the intermediate electronic structures as shown in Fig. 3. In Fig. 4 we can see it, as we have the band structures for all GBMLs illustrated in Fig. 1, with the expected diversity in the electronic structure of GBMLs, including metallic, semimetallic and semiconductor behaviour, shown.

The insertion of ELDs in GBMLs can generate C dangling bonds and consequently spin polarization (magnetic moment), thus giving

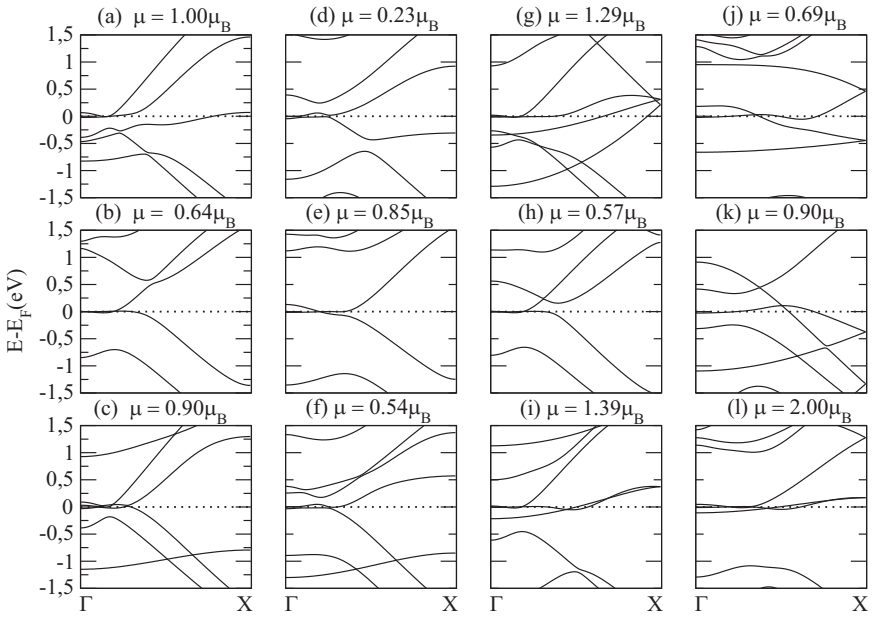

Fig. 5. Band structures of all ZGBNRs studied: (a) $ZGBNR_{8CN}$, (b) $ZGBNR_{8NN}$, (c) $ZGBNR_{8BN}$, (d) $ZGBNR_{8CC}$, (e) $ZGBNR_{8NC}$, (f) $ZGBNR_{8BC}$, (g) $ZGBNR_{4CN}$, (h) $ZGBNR_{4NN}$, (i) $ZGBNR_{4BN}$, (j) $ZGBNR_{4CC}$, (k) $ZGBNR_{4NC}$ and (l) $ZGBNR_{4BC}$.

rise to states at the Fermi level with the systems featuring as ferromagnetic metals (FM), as we can see from Figs. 4(a), (c), (g), (i) and (j). The GBMLs with 4-ELDs present induced edge states at ELD between domains of graphene and BC_2N.

The Figs. 1(b) and (h) present the same 558-ELD, but they possess different band structures being a semiconductor (4(b)) and a semimetal (4(h)), respectively. While $GBML_{8NN}$ (Fig. 1(b)) is perfectly flat, the $GBML_{4NN}$ (Fig. 1(h)) is not, with a larger domain of graphene. A similar behaviour was observed for $GBML_{8NC}$ (1(e)) and $GBML_{4NC}$ (1(k)). This shows that the shape and size of domains in GBMLs can tune its electronic properties. On the other hand, the GBMLs with no pending bonds ($GBML_{8NN}$, $GBML_{8CC}$, $GBML_{4NN}$, $GBML_{8BC}$ and $GBML_{4NC}$) present no magnetic moment, as can be seen in Figs. 1(b), (d), (e), (f) and (k). All these structures showed the band gaps listed in Table 1). It was seen that, depending on the type of defect and effect type-edge, the GBMLs can have semiconductor, metallic or semimetallic character. In our previous work [46], we showed that the insertion of 558 and 4 ELDs in graphene maintains its semimetallic character. The Figs. 4(d) and (j) show that graphene with BN domains and these types of defects can change the electronic properties of graphene from semimetal to semiconductor and metal respectively Fig. 5.

Zigzag BNC nanoribbons, which have an equal number of B, C and N atoms display a range of conduction properties, including half-metallic, metallic and semiconducting properties depending on the nature of edge passivation [47]. On the other hand Y. Liu et al. showed that the ferromagnetic, nonmagnetic, or certain ferrimagnetic state, the hybrid C-BN nanoribbons are all metallic [48]. We saw that ZGBNRs are always metallic with ferromagnetic coupling between carbon atoms edge (as seen in Figs. 2 and 5).

4. Conclusion

We have performed first principles calculations to study the structural, magnetic and electronic properties of hybrid GBMLs and ZGBNRs with ELDs. If the graphene and BC_2N domains are symmetric and the atoms are inserted into the grain boundary, the formation of an ELD with an octagonal ring (8-ELD) occurs and a reconstruction process is observed forming a ELD composed by two pairs of pentagonal rings surrounding one octagonal ring (558-ELD). If the graphene and BC_2N domains are antisymmetric and the atoms inserted into the grain boundary form an ELD with tetragonal ring (4-ELD), a different reconstruction process is observed forming 4-ELD, 558-ELD, and 8-ELD systems. The number of electrons at the grain boundaries influences in the ELDs reconstruction process. It was seen that, between GBMLs and ZGBNRs with ELDs, the $GBML_{8BN}$ and $ZGBNR_{8BN}$ are the most stable structures, both showing a 558-ELD, and maximizing the number of B-N bonds. Structures that have higher formation energies show a 4-ELD with C atoms remaining at the plane, being four coordinated flat and presenting strong compression.

The inclusion of these ELDs can create type-edge effects in the ELDs at GBNMLs, inducing spin polarization (magnetic moment) and creating states at the Fermi level. It was seen that, depending on the type of defect, existence of dangling bonds, and type-edge effect, the GBMLs can have semiconductor, metallic or semimetallic character. The shape and size of GBMLs domains can tune its electronic properties. Finally, we saw that ZGBNRs are always metallic with ferromagnetic coupling between edge carbon atoms.

Acknowledgements

We would like to thank the financial support given by the Brazilian Agencies, CNPq, INCT - Nanomateriais de Carbono, and CAPES.

References

[1] K.S. Novoselov, et al., Science 306 (2004) 666.
[2] L.A. Falkovsky, A.A. Varlamov, Phys. -Usp. 55 (2012) 1140.
[3] A.H.Castro. Neto, et al., Rev. Mod. Phys. 81 (2009) 109.
[4] L.A. Falkovsky, J. Phys. Conf. Ser. 129 (2008) 012004.
[5] C. Lee, X. Wei, J.W. Kysar, J. Hone, Science 321 (2008) 385.
[6] J. Baringhaus, et al., Nature 506 (2014) 349.
[7] R.R. Nair, et al., Science 320 (2008) 1308.
[8] X. Ma, H. Zhang, Nanoscale Res. Lett. 8 (2013) 440.
[9] G.Z. Magda, et al., Nature 514 (2014) 608.
[10] Y.-W. Son, M.L. Cohen, S.G. Louie, Phys. Rev. Lett. 97 (2007) 216803.
[11] K. Nakada, et al., Phys. Rev. B 54 (1996) 17954.
[12] W.Y. Kim, K.S. Kim, Nat. Nanotechnol. 3 (2008) 408.
[13] F. Muñoz-Rojas, J. Fernández-Rossier, J.J. Palacios, Phys. Rev. Lett. 102 (2009) 136810.
[14] L. Pisani, et al., Phys. Rev. B 75 (2007) 064418.
[15] M. Corso, et al., Science 303 (2004) 217.
[16] G. Cassabois, P. Valvin, B. Gil, Nat. Photon 10 (2016) 262.
[17] M. Topsakal, E. Aktürk, S. Ciraci, Phys. Rev. B 79 (2009) 115442.

[18] Z. Zhang, W. Guo, Phys. Rev. B 77 (2008) 075403.
[19] H. Zeng, et al., Nano Lett. 10 (2010) 5049.
[20] V.L. Solozhenko, et al., Appl. Phys. Lett. 78 (2001) 1385.
[21] H.A. Castillo, et al., Surf. Coat. Technol. 204 (2010) 4051.
[22] J. Lu, et al., Nat. Commun. 4 (2013) 2681.
[23] A.Y. Liu, W.M. Renata, M.L. Cohen, Phys. Rev. B 39 (1989) 1760.
[24] S. Azevedo, Eur. Phys. J. B 44 (2005) 203.
[25] P. Lu, Z. Zhang, W. Guo, J. Phys. Chem. C 115 (2010) 3572.
[26] Z. Liu, et al., Nat. Nanotechnol. 8 (2013) 119.
[27] J. Li, et al., Nano Lett. 14 (2014) 5133.
[28] D. Sanchez-Portal, et al., Int. J. Quantum Chem. 65 (1997) 435.
[29] J.M. Soler, et al., J. Phys.: Condens. Matter 14 (2002) 2745.
[30] P. Hohenberg, W. Kohn, Phys. Rev. B 136 (1964) B864.
[31] W. Kohn, L. Sham, Phys. Rev. Lett. 140 (1965) A1133.
[32] J.P. Perdew, S. Burke, M. Ernzerhof, Phys. Rev. Lett. 77 (1996) 3865.
[33] N. Troullier, J. Martins, Phys. Rev. B 43 (1991) 1993.
[34] L. Kleinman, M. Bylander, Phys. Rev. Lett. 48 (1982) 1425.
[35] S.S. Alexandre, H. Chacham, R.W. Nunes, Phys. Rev. B 63 (2001) 045402.
[36] J.P. Guedes, S. Azevedo, M. Machado, Eur. Phys. J. B 80 (2011) 127.
[37] L.C. Gomes, et al., Phys. Chem. C 117 (2013) 11770.
[38] J. Lahiri, et al., Nat. Nanotechnol. 5 (2010) 326.
[39] J.-H. Chen, et al., Phys. Rev. B 89 (2014) 121407 (R).
[40] H. Braunschweig, et al., Science 336 (2012) 1420.
[41] H. Nozaki, S. Itoh, J. Phys. Chem. Solids 57 (1996) 41.
[42] Y. Li, et al., Nanoscale 4 (2012) 2580.
[43] T. Guerra, S. Azevedo, M. Machado, Solid State Commun. 234–235 (2016) 45.
[44] E.H. Lieb, Phys. Rev. Lett. 62 (1989) 1201.
[45] H. González-Herrero, et al., Science 352 (2016) 437.
[46] T. Guerra, S. Azevedo, M. Machado Eur, Phys. J. B 89 (2016) 58.
[47] E.A. Basheer, P. Parida, S.K. Pati, New J. Phys. 13 (2011).
[48] Y. Liu, et al., J. Phys. Chem. C 115 (2011) 9442.